

# Magnetic-field induced superconductor-metal-insulator transitions in bismuth metal-graphite

Masatsugu Suzuki,\* Itsuko S. Suzuki, and Robert Lee

*Department of Physics, State University of New York at Binghamton, Binghamton, New York 13902-6016*

Jürgen Walter

*Department of Materials Science and Processing, Graduated School of Engineering,  
Osaka University, 2-1, Yamada-oka, Suita, 565-0879, JAPAN*

(Dated: November 3, 2018)

Bismuth-metal graphite (MG) has a unique layered structure where Bi nanoparticles are encapsulated between adjacent sheets of nanographites. The superconductivity below  $T_c$  ( $= 2.48$  K) is due to Bi nanoparticles. The Curie-like susceptibility below 30 K is due to conduction electrons localized near zigzag edges of nanographites. A magnetic-field induced transition from metallic to semiconductor-like phase is observed in the in-plane resistivity  $\rho_a$  around  $H_c$  ( $\approx 25$  kOe) for both  $H \perp c$  and  $H \parallel c$  ( $c$ :  $c$  axis). A negative magnetoresistance in  $\rho_a$  for  $H \perp c$  ( $0 < H \leq 3.5$  kOe) and a logarithmic divergence in  $\rho_a$  with decreasing temperature for  $H \parallel c$  ( $H > 40$  kOe) suggest the occurrence of two-dimensional weak localization effect.

PACS numbers: 71.24.+q, 74.80.Dm, 72.15.Rn, 71.30.+h

## I. INTRODUCTION

A weak localization theory predicts a logarithmic divergence of the resistivity in the two-dimensional (2D) electron systems as the temperature ( $T$ ) is lowered.<sup>1</sup> In high-mobility Si metal oxide-semiconductor field-effect transistor (MOSFET), the in-plane resistivity for a system with an electron density  $n$  larger than a critical electron density  $n_c$  decreases with decreasing  $T$ , indicating a metallic behavior.<sup>2,3,4</sup> This metallic state is completely destroyed by the application of an external magnetic field ( $H$ ) applied in the basal plane when  $H$  is higher than a threshold field  $H_c$ . Such coplanar fields only polarize the spins of the electrons, indicating that the spin state is significant to the high conductivity of the metallic state. The scaling relation of the in-plane resistivity collapses into two distinct branches above and below  $H_c$ . Such behaviors are very similar to those observed in amorphous ultrathin metal films of  $\text{InO}_x$ ,<sup>5</sup>  $\text{MoGe}$ ,<sup>6,7</sup> and  $\text{Bi}$ ,<sup>8</sup> which undergo magnetic field-induced transitions from superconducting phase to insulating phase.

Bi-metal graphite (MG) constitutes a novel class of materials having unique layered structures. This system can be prepared from the reduction by Li-diphenylide from an acceptor-type  $\text{BiCl}_3$  graphite intercalation compound (GIC) as a precursor material. Ideally, the staging structure of Bi-MG would be the same as that of  $\text{BiCl}_3$  GIC.<sup>9,10,11</sup> In Bi-MG, Bi atoms would form intercalate layers sandwiched between adjacent graphite layers. For the stage- $n$  ( $= 1, 2, \dots$ ) structure, the packages of  $n$  graphite layers and one Bi layer would be periodically stacked along the  $c$  axis perpendicular to the graphite basal plane. In  $\text{BiCl}_3$  GIC, the ratio of  $c$ -axis resistivity  $\rho_c$  to the in-plane resistivity  $\rho_a$  ( $\Delta = \rho_c/\rho_a$ ) at room temperature is  $(7.4 - 4.9) \times 10^3$ ,<sup>11</sup> suggesting that virtually all  $\pi$ -electrons are directionally localized; i.e., they can move freely along the graphite basal planes,

but are unable to diffuse across the stack of layers.<sup>12</sup> Such a large ratio  $\Delta$  is due to the insulating  $\text{BiCl}_3$  layer sandwiched between the adjacent graphite layers. There is no overlapping of the wave functions over nearest neighbor graphite layers. The situation may not drastically change in Bi-MG in spite of the fact that  $\text{BiCl}_3$  layer is replaced by metallic Bi layer. In fact the  $c$ -axis resistivity of Bi-MG ( $= 0.1 \Omega\text{cm}$  at 298 K) is almost the same as that of  $\text{BiCl}_3$  GIC at the same  $T$ , suggesting that Bi-MG behaves like a quasi 2D conductor.

In this paper we have undertaken an extensive study on the transport and magnetic properties of Bi-MG. We show that this compound undergoes a superconducting transition at  $T_c = 2.48$  K. A magnetic-field induced transition from metallic to semiconductor-like phase is observed in  $\rho_a$  around  $H \approx 25$  kOe for  $H \perp c$  and  $H \parallel c$  ( $c$ :  $c$  axis). These results of Bi-MG are compared with those of Si MOSFET, and amorphous ultrathin metal films of  $\text{InO}_x$ ,<sup>5</sup>  $\text{MoGe}$ ,<sup>6,7</sup> and  $\text{Bi}$ .<sup>8</sup>

Structural studies of Bi-MG reveal that Bi layers are formed of Bi nanoparticles which are encapsulated between adjacent sheets of nanographites. The size of nanographites in Bi-MG is much smaller than the in-plane coherence size of the graphite layers of pristine graphite. The superconductivity is mainly due to Bi nanoparticles, while the magnetism is mainly due to nanographites. Nanographites are nanometer-sized graphite fragments which represent a new class of mesoscopic system intermediate between aromatic molecules and extended graphene sheets. Fujita and co-workers<sup>13,14,15</sup> have theoretically suggested that the electronic structures of finite-size graphene sheets depend crucially on the shape of their edges. The graphene edge of an arbitrary shape consists of two-types of edges, zigzag type and armchair type. The former has a transpolyacetylene type structure and the latter has a cispolyacetylene one. Finite graphite systems having zigzag

edges exhibit a special edge state. The corresponding energy bands are almost flat at the Fermi energy, thereby giving a sharp peak in the density of states (DOS) at the Fermi energy. This is in contrast to the case of 2D graphene sheet with infinite size, where the DOS is zero at the Fermi energy. According to Wakabayashi et al.,<sup>15</sup> the magnetism of nanographites is characterized by Pauli paramagnetism and orbital diamagnetism from conduction electrons. They have predicted that the Pauli paramagnetic susceptibility for the nanographites with zigzag edges shows a Curie-like behavior at low temperatures, which is in contrast to a  $T$ -independent Pauli paramagnetism in normal metals. In this paper we show that the susceptibility of Bi-MG has a Curie-like behavior at low  $T$ . This behavior is discussed in the light of the prediction by Wakabayashi et al.<sup>15</sup>

## II. EXPERIMENTAL PROCEDURE

BiCl<sub>3</sub> GIC samples as a precursor material, were prepared by heating a mixture of highly oriented pyrolytic graphite (HOPG) [grade ZYA from Advanced Ceramics, Ohio] and an excess amount of BiCl<sub>3</sub> at 200 °C in a ampoule filled with chlorine gas at a pressure of 375 Torr.<sup>9,10</sup> The reaction was continued for three days. It was confirmed from (00 $L$ ) x ray diffraction (Rigaku RINT 2000 x-ray powder diffractometer) that the BiCl<sub>3</sub> GIC sample consists of stage-2 as majority phase and stage-3 and stage-4 as minority phase. The  $c$  axis repeat distance is  $13.17 \pm 0.05$  Å for stage-2,  $15.85 \pm 0.25$  Å for stage-3, and  $20.22 \pm 0.25$  Å for stage-4, respectively. No Bragg reflection from the pristine graphite is observed.

The synthesis of Bi-MG was made by the reduction by Li-diphenylide from BiCl<sub>3</sub> GIC. BiCl<sub>3</sub> GIC samples were kept for three days in a solution of lithium diphenylide in tetrahydrofuran (THF) at room temperature. Then the samples were filtered, rinsed by THF, and dried in air. Finally the samples were annealed at 260 °C in a hydrogen gas atmosphere for one day. The structure of Bi-MG thus obtained was examined by (00 $L$ ) x-ray diffraction, and bright field images and selected-area electron diffraction (SAED) (Hitachi H-800 transmission electron microscope) operated at 200 kV. The same methods for the structural analysis were used for Pd-MG.<sup>16,17,18</sup> The (00 $L$ ) x-ray diffraction pattern of Bi-MG is much more complicated than that of BiCl<sub>3</sub> GIC, which makes it difficult to calculate the average particle thickness from the identity period in Bi-MG. Note that graphite reflections appear in Bi-MG, suggesting that a part of Bi atoms leaves from the graphite galleries occupied by BiCl<sub>3</sub> intercalate layers in BiCl<sub>3</sub> GIC during the reduction process. Such Bi atoms tend to form multilayered Bi nanoparticles in the graphite galleries in Bi-MG. The number of Bi layers in possible multilayered structures could not be exactly determined at present. SAED pattern of Bi-MG consists of polycrystalline diffraction rings, suggesting that there are at least four Bi layers in thickness. Re-

TABLE I: Experimentally observed spacings  $d_{exp}$  for Bi-MG and  $d_{PDF}$  given by powder diffraction file (PDF) 5-0519 for rhombohedral Bi [spacegroup: R-3m ( $a_0 = 4.546$  Å,  $c_0 = 11.860$  Å for the notation of the hexagonal close-packed structure)]. All reflections can be indexed as ( $hkl$ ) reflections of Bi. Graphite reflections are not included.

$d_{exp}$ (Å)	$d_{PDF}$ (Å)	( $hkl$ )
3.24	3.28	102
2.35	2.39	014
1.92	1.970	113
1.71	1.868	022
1.51	1.515	025
1.40	1.443	212

flections from Bi and graphite were observed. As listed in Table I, all the Bi reflections were labeled and attributed to the formation of rhombohedral Bi, according to the standard ICDD PDF (Card No. 05-0519). This result indicates that Bi nanoparticles are crystallized as rhombohedral Bi phase in Bi-MG. The observed spacings of Bi-MG are 1-2 % shorter than those of bulk Bi metal. The size of Bi nanoparticles distribute widely around the average size 110 Å. More than 50 % of Bi nanoparticles has sizes ranging between 10 and 50 Å. The largest particle size is 750 Å.

The measurements of DC magnetization and resistivity were made using a SQUID magnetometer (Quantum Design MPMS XL-5) with an ultra low field capability and an external device control mode. In the present work we used a Bi-MG sample based on HOPG which is partially exfoliated. The stoichiometry of C and Bi was not determined. The in-plane resistivity  $\rho_a$  and the  $c$  axis resistivity  $\rho_c$  were measured by a conventional four-probe method. The sample had a rectangular form with a base  $6.0 \times 1.6$  mm<sup>2</sup> and a height 0.47 mm along the  $c$  axis. For the measurement of  $\rho_a$ , four thin gold wires (25- $\mu$ m diameter) that were used as the current and voltage probes were attached to one side of the  $c$  surfaces by silver paste (4922N, du Pont). For the measurement of  $\rho_c$ , two thin gold wires as the current and voltage probes were attached to each  $c$ -surface of the sample. The current ( $I = 10$  mA for  $\rho_a$  and 3 mA for  $\rho_c$ ) was supplied through the current probes by a Keithley type 224, programmable DC current source. The voltage  $V$  generated across the voltage probes was measured by a Keithley 182 nanovoltmeter. The linearity of  $I$ - $V$  characteristics was confirmed for the measurements of  $\rho_a$  and  $\rho_c$ .

## III. RESULT AND DISCUSSION

### A. Meissner effect due to Bi nanoparticles

We measured the DC magnetization of Bi-MG. After the sample was cooled from 298 to 1.9 K at  $H = 0$ , the

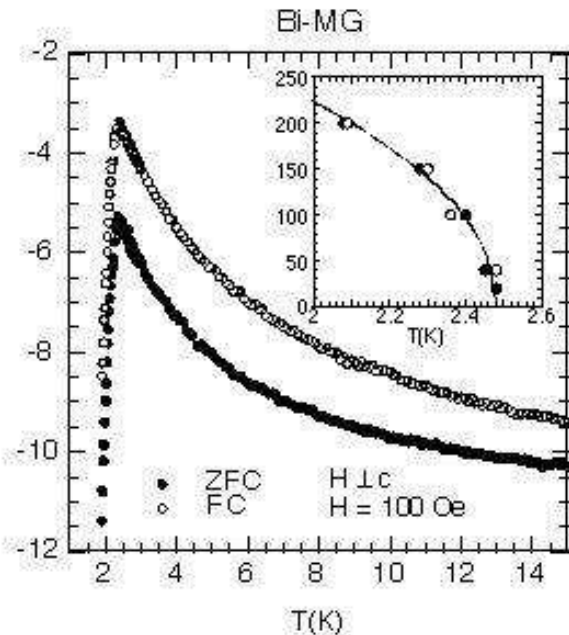


FIG. 1:  $T$  dependence of ZFC and FC susceptibilities of Bi-MG based on HOPG.  $H = 100$  Oe.  $H \perp c$  ( $c$ :  $c$  axis). The inset shows the magnetic phase diagram of  $H$  vs  $T$  for  $H \perp c$ , where the peak temperatures of ZFC and FC susceptibilities are plotted as a function of  $H$ . The solid line denotes the least-squares fit of the ZFC data ( $\bullet$ ) to Eq.(1).

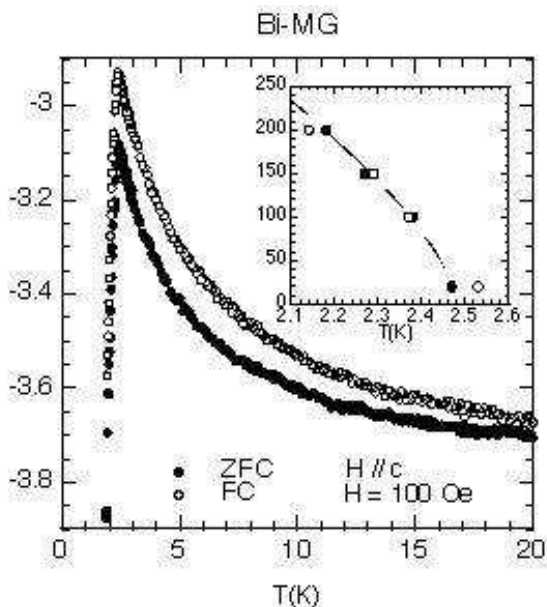


FIG. 2:  $T$  dependence of ZFC and FC susceptibilities of Bi-MG.  $H = 100$  Oe.  $H \parallel c$  ( $c$ :  $c$  axis). The inset shows the magnetic phase diagram of  $H$  vs  $T$  for  $H \parallel c$ . The solid line denotes the least-squares fitting curve for the ZFC data ( $\bullet$ ) to Eq.(1).

measurement of zero field cooled (ZFC) magnetization  $M_{ZFC}$  was made with increasing  $T$  from 1.9 to 15 K in the presence of  $H$ . The sample was kept for 20 minutes at 50 K. Then the sample was cooled from 50 to 15 K. The measurement of field-cooled (FC) magnetization  $M_{FC}$  was made with decreasing  $T$  from 15 to 1.9 K in the presence of the same  $H$ . For convenience, hereafter, the direction of  $H$  in the  $c$  plane is denoted as  $H \perp c$  ( $c$ :  $c$  axis). Figures 1 and 2 show typical examples of the  $T$  dependence of the susceptibility  $\chi_{ZFC}$  ( $=M_{ZFC}/H$ ) and  $\chi_{FC}$  ( $=M_{FC}/H$ ) at  $H = 100$  Oe for  $H \perp c$  and  $H \parallel c$ , respectively. Both  $\chi_{FC}$  and  $\chi_{ZFC}$  show a sharp peak around 2.5 K at  $H = 20$  Oe, which results from the competition between the diamagnetic susceptibility due to the Meissner effect and the Curie-like susceptibility (which will be described later). The peak shifts to the low  $T$  side with increasing  $H$ . No peak is observed above 1.9 K for  $H \geq 250$  Oe. For convenience, the peak temperature is defined as a critical temperature  $T_c(H)$ . The peak temperature  $T_c(H)$  for  $\chi_{FC}$  is almost the same as that for  $\chi_{ZFC}$ . In the insets of Figs. 1 and 2, we show the  $H$ - $T$  magnetic phase diagram for Bi-MG for  $H \perp c$  and  $H \parallel c$ , respectively. We find that the data of  $H$  vs  $T$  (ZFC susceptibility) for  $H \perp c$  and  $H \parallel c$  are well described by

$$H = H_0 \left( \frac{T_c - T}{T_c} \right)^\beta, \quad (1)$$

where  $H_0$  is the critical field at  $T = 0$  K ( $H_0 = H_{c2}$  for  $H \perp c$  and  $H_0 = H_{c3}$  for  $H \parallel c$ ),  $\beta$  is an exponent, and  $T_c$  is a critical temperature at  $H = 0$ . The field  $H_{c3}$  is a field to nucleate a small superconducting region near the sample surface. The least squares fits of the data of  $H$  vs  $T$  (ZFC susceptibility) yield the values of  $H_{c2} = 489.4 \pm 0.5$  Oe,  $\beta = 0.48 \pm 0.02$ ,  $T_c = 2.48 \pm 0.06$  K for  $H \perp c$ , and  $H_{c3} = 838 \pm 1$  Oe,  $\beta = 0.69 \pm 0.02$ ,  $T_c = 2.48 \pm 0.02$  K for  $H \parallel c$ . Here we note that the superconductivity is observed in ultrathin films of amorphous Bi grown in top of layer of amorphous Ge (thickness, 6 - 10 Å). Haviland et al.<sup>19</sup> have reported that the superconductivity occurs for the thickness of Bi films,  $d = 6.73 - 74.27$  Å. The critical temperature  $T_c$  decreases with decreasing  $d$ :  $T_c = 5.6$  K for  $d = 74.27$  Å and  $T_c \approx 0.8$  K for  $d \approx 6.73$  Å. Markovic et al.<sup>8</sup> have shown that  $T_c$  decreases with decreasing  $d$  for  $d > d_c$  ( $d_c = 12.2$  Å):  $T_c = 0.5$  K for  $d = 15$  Å. Weitzel and Micklitz<sup>20</sup> have reported surface superconductivity in granular films built from well-defined rhombohedral Bi clusters (mean size = 38 Å) embedded in difference matrices (Kr, Xe, Ge) or with  $H_2$  or  $O_2$  gas adsorbed on the cluster surface. The critical temperature  $T_c$ , which is dependent on matrices and gases used, is between 2 and 6 K. This value of  $T_c$  is on the same order as that of Bi-MG. The exponent  $\beta$  for  $H \perp c$  is very close to that ( $\beta = 0.5$ ) predicted for homogeneous system of isolated superconducting grains.<sup>21</sup> The ratio  $H_{c3}/H_{c2}$  is calculated as 1.71, which is very close to the predicted value 1.695.<sup>22</sup> Similar behavior is observed in the critical fields for  $H \perp c$  and  $H \parallel c$  in stage-1 K GIC (KC<sub>8</sub>).<sup>23</sup> The

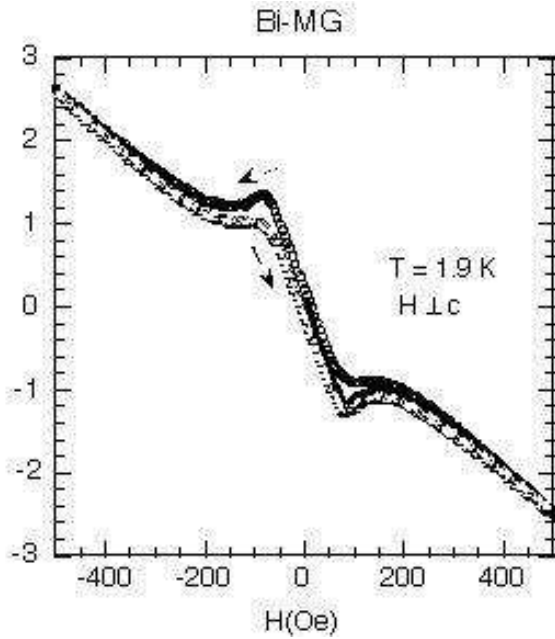


FIG. 3: Hysteresis loop of DC magnetization for Bi-MG.  $H \perp c$ .  $T = 1.9$  K. The measurement was made with increasing  $H$  from 0 to 500 Oe (denoted by  $\bullet$ ), with decreasing  $H$  from 500 Oe to -500 Oe ( $\circ$ ), and with increasing  $H$  from -500 Oe to 500 Oe ( $\Delta$ ).

coherence length  $\xi$  is estimated as  $\xi = 820 \text{ \AA}$  from the value of  $H_{c2}$  using the relation  $H_{c2} = \Phi_0 / (2\pi\xi^2)$ , where  $\Phi_0 (= 2.0678 \times 10^{-7} \text{ Gauss cm}^2)$  is a fluxoid. The coherence length  $\xi$  is much larger than the size of islands ( $110 \text{ \AA}$  in average).

Figure 3 shows the hysteresis loop of the magnetization  $M_a(H)$  for  $H \perp c$  at  $T = 1.9$  K. The sample was cooled from 298 K to 1.9 K at  $H = 0$ . The magnetization  $M_a(H)$  was measured with increasing  $H$  from 0 to 500 Oe, with decreasing  $H$  from 500 Oe to -500 Oe, and with increasing  $H$  from -500 Oe to 500 Oe. The magnetization consists of superconductivity contribution and diamagnetic background. In Fig. 4(a) we show the hysteresis loop of  $\Delta M_a(H)$  that is defined by  $M_a(H)$  at 1.9 K minus a diamagnetic background given by  $\chi_d H$  with  $\chi_d = -5.143 \times 10^{-7} \text{ emu/gOe}$ . A hysteresis loop characteristic to a type-II superconductor is observed with a lower critical field  $H_{c1}$  ( $= 80$  Oe). In contrast, the magnetization hysteresis loop  $M_a(H)$  at  $T = 3.3$  K is very different from that at 1.9 K. It seems that there is neither local minimum nor local maximum. In Fig. 4(b) we show the hysteresis loop of  $\Delta M_a(H)$  which is defined by at  $M_a(H)$  at 3.3 K minus a diamagnetic background given by  $\chi_d H$  with  $\chi_d = -7.317 \times 10^{-7} \text{ emu/gOe}$ . As  $H$  decreases, a trapped magnetic flux, corresponding to a paramagnetic moment  $M_r$  ( $\approx 2.7 \times 10^{-5} \text{ emu/g}$ ) remains in the sample. With further cycling of  $H$  from -500 to 500 Oe a characteristic hysteresis loop is observed.

We also measured the hysteresis loop of the magnetization  $M_c(H)$  for  $H \parallel c$  at  $T = 1.9$  K. The difference  $\Delta M_c$

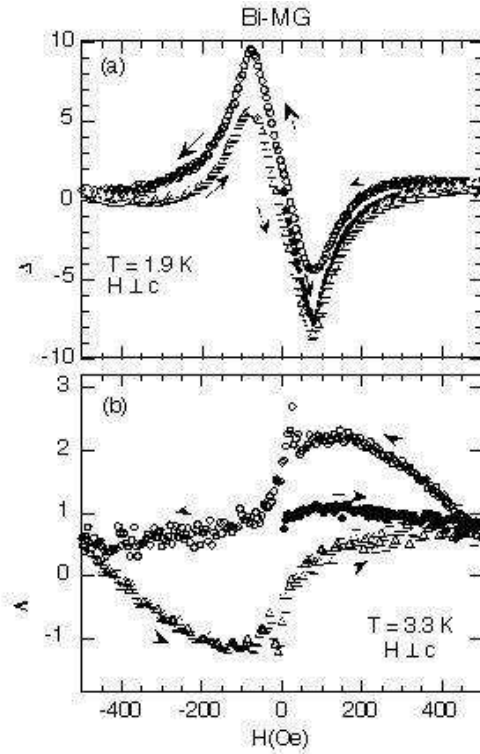


FIG. 4: Hysteresis loop of DC magnetization minus a diamagnetic background ( $= \chi_d H$ ) for Bi-MG.  $H \perp c$ . (a)  $T = 1.9$  K.  $\chi_d = -5.143 \times 10^{-7} \text{ emu/gOe}$ . (b)  $T = 3.3$  K.  $\chi_d = -7.317 \times 10^{-7} \text{ emu/gOe}$ .

is defined by  $M_c(H)$  at 1.9 K minus a diamagnetic background given by  $\chi_d H$  with  $\chi_d = -2.980 \times 10^{-6} \text{ emu/gOe}$ . The hysteresis loop of  $\Delta M_c$  for  $H \parallel c$  is very similar to the corresponding data  $\Delta M_a$  for  $H \perp c$ . The value of  $H_{c1}$  ( $= 75$  Oe) for  $H \parallel c$  is a little lower than that for  $H \perp c$ . The peak value of  $\Delta M_c$  is almost the same as that of  $\Delta M_a$ . The hysteresis loop of  $\Delta M_c$  at 1.9 K exhibits a nearly reversible behavior. In bulk samples this could be explained in terms of a lack of structural defects to provide pinning sites in the vortex state ( $H_{c1} < H < H_{c2}$ ). In Bi-MG, however, the size of islands is much shorter than the coherence length  $\xi$ . Thus the pinning effect is not relevant for these islands. In contrast, the hysteresis loop of  $\Delta M_a$  at 1.9 K exhibits some hysteretic behavior. Note that similar magnetization curves are observed in a superconductor TaC nanoparticles which are synthesized using a vapor-solid reaction path starting with carbon nanotube precursor.<sup>24</sup>

## B. Curie-like susceptibility due to nanographites

Figure 5 shows typical data of  $\chi_{FC}$  for  $H = 1$  kOe for  $H \perp c$  and  $H \parallel c$ . The susceptibility is negative at high  $T$  and drastically increases with decreasing  $T$ . The least squares fit of the data ( $\chi_{FC}$  vs  $T$ ) for  $1.9 \leq T \leq 30$  K to

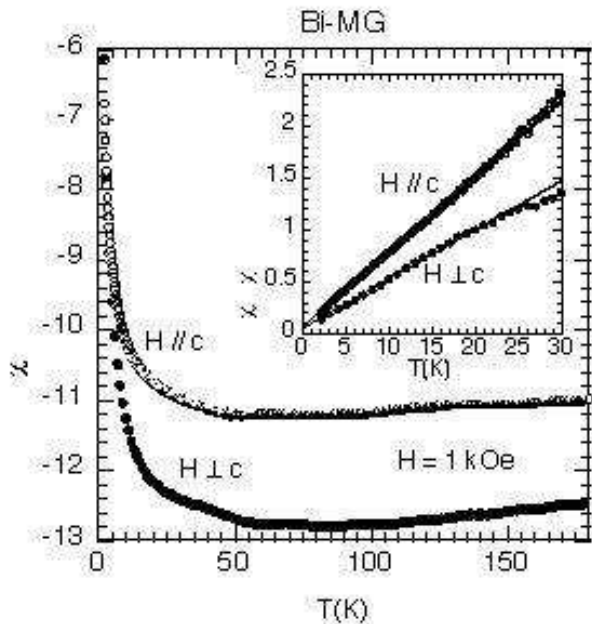


FIG. 5:  $T$  dependence of FC susceptibilities for Bi-MG.  $H = 1$  kOe.  $H \perp c$  and  $H \parallel c$ . The inset shows the reciprocal susceptibility  $(\chi - \chi_0)^{-1}$  as a function of  $T$ . The solid lines are described by Eq.(2) with parameters given in the text.

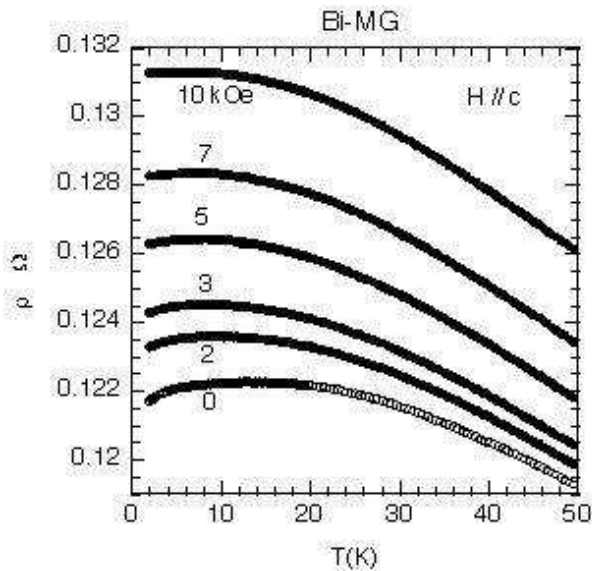


FIG. 6:  $T$  dependence of  $c$ -axis resistivity  $\rho_c(T, H)$  for Bi-MG at various  $H$ .  $H \parallel c$ .  $I \parallel H$ .

the Curie-Weiss law

$$\chi = \chi_0 + \frac{C}{T - \Theta}, \quad (2)$$

yields  $\Theta = -0.86 \pm 0.05$  K,  $C = (1.999 \pm 0.029) \times 10^{-6}$  emu K/g,  $\chi_0 = (-1.307 \pm 0.001) \times 10^{-6}$  emu/g for  $H \perp c$ , and  $\Theta = -1.13 \pm 0.02$  K,  $C = (1.460 \pm 0.008) \times 10^{-6}$  emu K/g,  $\chi_0 = (-1.146 \pm 0.001) \times 10^{-6}$  emu/g for  $H \parallel c$ . The

value of  $\Theta$  is very close to zero, showing a Curie-like law. In the inset of Fig. 5 we show the reciprocal susceptibility  $(\chi - \chi_0)^{-1}$  as a function of  $T$ . The negative value  $\chi_0$  is from the orbital diamagnetic susceptibility. There is a crossover from the high-temperature diamagnetic susceptibility to the low-temperature Curie-like susceptibility around 50 K. We assume that the susceptibility of Bi-MG at 100 K corresponds to the diamagnetic susceptibility since the Pauli susceptibility is positive and is nearly equal to zero at 100 K. From Fig. 5 the diamagnetic susceptibility for  $H \parallel c$  and  $H \perp c$  is estimated as  $\chi_c \approx -1.1 \times 10^{-6}$  emu/g and  $\chi_a \approx -1.3 \times 10^{-6}$  emu/g, which are almost isotropic. These values are in contrast with the susceptibility of HOPG, which is very anisotropic:  $\chi_c = -25.86 \times 10^{-6}$  emu/g and  $\chi_a = -1.06 \times 10^{-7}$  emu/g at  $H = 1$  kOe. The absolute value of  $\chi_c$  in Bi-MG is much smaller than that in HOPG, while the values of  $\chi_a$  are on the same order for both systems.

Here it is interesting to compare our data of susceptibility with that of nanographites prepared by heat treating diamond nanoparticles<sup>25</sup> and a disorder network of nanographites in activated carbon fiber (ACF).<sup>26</sup> The  $T$  dependence of the susceptibility for these compounds is similar to that of Bi-MG. In particular, the values of  $\Theta$ ,  $C$ , and  $\chi_0$  for the ACF are on the same order as those for Bi-MG, where  $\Theta \approx -2$  K,  $C = 1.21 \times 10^{-6}$  emu K/g, and  $\chi_0 = -1.36 \times 10^{-6}$  emu/g for ACF prepared at the heat treatment temperature  $\text{HTT} = 1500$  °C.<sup>26</sup> Here we assume that the spin  $S$  is  $1/2$  and the Landé  $g$ -factor is 2 since the spins are associated with carbon materials. The number of spin density per 1 g of Bi-MG is estimated as  $(4.7 - 6.4) \times 10^{18}$ /g, which is comparable with  $3.9 \times 10^{18}$ /g for the ACF with  $\text{HTT} = 1500$  °C.<sup>26</sup>

It has been theoretically predicted by Wakabayashi et al.<sup>15</sup> that the Pauli susceptibility exhibits a Curie-like behavior in the nanographites with zigzag edges, because of the DOS which is sharply peaked at the Fermi energy. However, qualitatively we think that the Curie-like behavior at low  $T$  in Bi-MG is due to the conduction electrons localized around the zigzag edges of nanographites, which have local magnetic moments (spin  $S = 1/2$  and a Landé  $g$ -factor  $g = 2$ ). The origin of spin polarization in nanographites with zigzag edges has been discussed by Fujita et al.<sup>13</sup> using the Hamiltonian that consists of the on-site Coulomb repulsive interaction ( $U$ ) when the site is occupied by two electrons, and the electron transfer integral between the nearest sites ( $t$ ). They have shown that a ferrimagnetic spin polarization emerges on the edge carbons even for weak  $U/t \approx 0.1$ .

The orbital diamagnetic susceptibility is very sensitive to the size and edge shapes of nanographites. The orbital diamagnetic susceptibility is almost isotropic in Bi-MG, while it is very anisotropic in pristine graphite with infinite size. In Bi-MG the orbital cyclotron motion of electrons in the presence of  $H$  ( $H \parallel c$ ) is greatly suppressed. This result is in good agreement with the prediction by Wakabayashi et al.<sup>15</sup> In ribbon-shaped nanographites with zigzag edges, the magnitude of the diamagnetic sus-

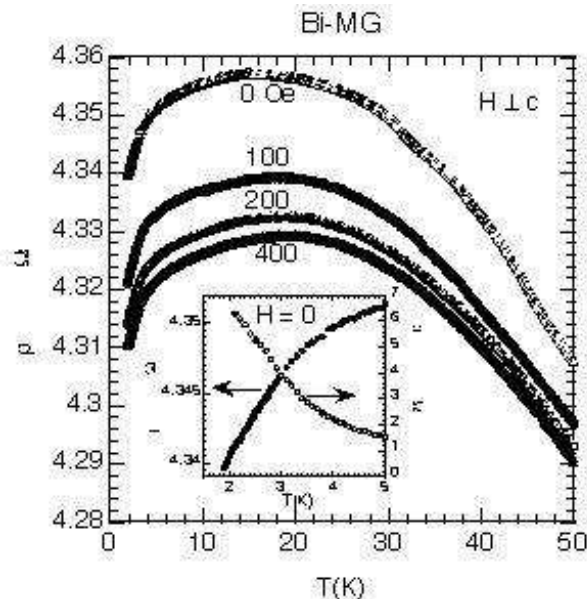


FIG. 7:  $T$  dependence of in-plane resistivity  $\rho_a(T, H)$  for Bi-MG at  $H = 0, 100, 200,$  and  $400$  Oe.  $H \perp c$ .  $I \perp H$ . The inset shows the  $T$  dependence of  $\rho_a(T, H = 0)$  ( $\bullet$ ) and  $d\rho_a(T, H = 0)/dT$  ( $\circ$ ) at low  $T$ .

ceptibility decreases as the ribbon width decreases. The flow of the orbital diamagnetic ring current significantly depends on the lattice topology near the graphite edge.

### C. $c$ -axis and in-plane resistivities

The  $c$ -axis resistivity  $\rho_c$  of Bi-MG was measured using the four-probe method. After the sample was cooled from 298 K to 1.9 K at  $H = 0$ , the  $c$ -axis resistivity  $\rho_c$  was measured with increasing  $T$  from 1.9 K to 50 K without and with  $H$  [ $H \parallel c$  ( $c$ :  $c$  axis)], where the current direction is parallel to the field direction. This resistivity is denoted as the longitudinal magnetoresistance. Figure 6 shows the  $T$  dependence of  $\rho_c$  for Bi-MG at  $H = 0 - 10$  kOe. The resistivity  $\rho_c$  for Bi-MG shows a very broad peak around 14 K at  $H = 0$ , in contrast to  $\rho_c$  for HOPG exhibiting a peak around 40 K.<sup>12</sup> This peak shifts to the low  $T$  side with increasing  $H$ . For  $H \geq 20$  kOe,  $\rho_c$  shows a semiconductor-like behavior: it decreases with increasing  $T$ . Note that  $\rho_c$  shows a positive magnetoresistance: it increases with increasing  $H$  at any fixed  $T$  between 1.9 and 50 K. The value of  $\rho_c$  at  $T = 298$  K and  $H = 0$  is 0.11  $\Omega\text{cm}$ , which is on the same order as that of HOPG ( $\rho_c = 0.096$   $\Omega\text{cm}$ )<sup>12</sup> and BiCl<sub>3</sub> GIC ( $\rho_c = 0.2$   $\Omega\text{cm}$ ),<sup>11</sup> leading to a mean free path less than 1  $\text{\AA}$  according to the Drude formula. This result suggests that there is no overlapping over nearest-neighbor layers along the  $c$  axis. The  $c$ -axis conduction can occur via the hopping of carriers between layers.

The in-plane resistivity  $\rho_a$  of Bi-MG was also measured using the four-probe method. After the sample

was cooled from 298 K to 1.9 K at  $H = 0$ , the in-plane resistivity  $\rho_a$  was measured with increasing  $T$  from 1.9 K to 50 K without and with  $H$  ( $H \perp c$ ), where the field direction is perpendicular to the current direction in the  $c$  plane. This resistivity is denoted as the transverse magnetoresistance. The resistivity ratio  $\Delta (= \rho_c/\rho_a)$  is estimated as 30 at 298 K using the measured  $\rho_a$ . However, the actual value of  $\Delta$  is considered to be much larger than 30 because of possible contribution of  $\rho_c$  to the measured  $\rho_a$ . Figure 7 shows the  $T$  dependence of  $\rho_a$  of Bi-MG at  $H = 0 - 400$  Oe. The zero-field ( $H = 0$ ) in-plane resistivity increases with increasing  $T$  at low  $T$ , showing a metallic behavior. It has a maximum around 15 K, and it decreases with further increasing  $T$ , showing a semiconductor-like behavior. Note that the value of  $\rho_a$  for Bi-MG ( $= 4.2$   $\text{m}\Omega\text{cm}$ ) is much larger than that of BiCl<sub>3</sub> GIC ( $= 27$   $\mu\Omega\text{cm}$  at 298 K). We find that the  $T$  dependence of  $\rho_a$  for Bi-MG is very similar to that of grafoil: they even have similar magnitudes. The grafoil is a pyrolytic graphite with a polycrystalline structures formed of many domains. According to Koike et al.,<sup>27</sup>  $\rho_a$  of grafoil (grade GTA, Union carbide) shows a semiconductor-like behavior, while  $\rho_a$  of HOPG (Union Carbide) shows a metallic behavior. This result suggests that the semiconductor-like behavior in Bi-MG may arise from nanographites where the degree of disorder is greatly enhanced. Such a semiconductor-like behavior is observed at least below 25 kOe.

In the inset of Fig. 7 we show the detail of  $\rho_a$  at  $H = 0$  near  $T_c = 2.48$  K. No drastic decrease in  $\rho_a$  below  $T_c$  is observed with decreasing  $T$ , while the  $T$ -derivative  $d\rho_a/dT$  gradually decreases with increasing  $T$  around  $T_c$ . The causes for the finite value of  $\rho_a$  below  $T_c$  in spite of the superconducting phase are as follows. (i) The sample used in the present work is an exfoliated Bi-MG based on HOPG. The sample surface is not flat partly because of cracks generated in the basal plane. Since the current path is not always located on the same layer, the contribution of large  $\rho_c$  to the observed  $\rho_a$  is not negligibly small. Another possibility is the local superconductivity in isolated islands. In such a system there is competition between the Josephson coupling ( $E_J$ ) and the charging energy ( $E_U$ ) between superconducting islands.<sup>28</sup> For  $E_J \gg E_U$ , the Cooper pairs are delocalized leading to a superconducting state with vanishing resistivity. For  $E_J \ll E_U$ , the pairs will be localized and the transport is possible only by thermal activation leading to insulating behavior at  $T = 0$  K. The resistivity varies with  $T$  as  $\rho \approx \exp(T_a/T)$ , where  $T_a$  is related to the activation energy. In this model, the resistivity should increase with decreasing  $T$ , which contradicts with our result. Liu et al.<sup>29</sup> have reported an unusual  $T$  dependence of resistivity at low  $H$  in ultrathin superconducting films of Pb, Al, and Bi. The resistivity varies with  $T$  as  $\rho \approx \exp(T/T_0)$  at low  $T$ , where  $T_0$  is a characteristic temperature. In Bi-MG,  $d\rho/dT$  decreases with increasing  $T$  around  $T_c$ . In superconducting thin films,  $d\rho/dT [\approx \exp(T/T_0)/T_0]$  increases with increasing  $T$ . Therefore, the  $T$  dependence

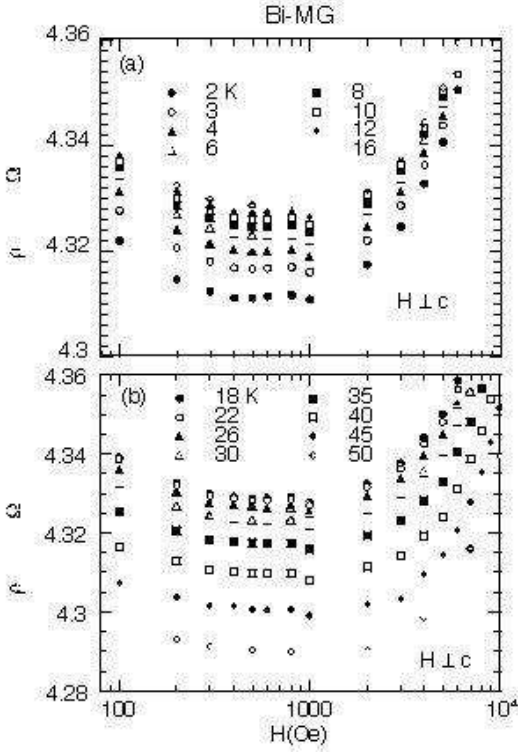


FIG. 8:  $H$  dependence of  $\rho_a(T, H)$  for Bi-MG at fixed  $T$  ( $2 \leq T \leq 50$  K).  $H \perp c$ .

of  $\rho_a$  in Bi-MG is not the case of  $\rho \approx \exp(T/T_0)$ .

#### D. 2D Weak localization effect

As shown in Fig. 7, the in-plane resistivity  $\rho_a$  slightly decreases with increasing  $H$  at the same  $T$  (at least for  $1.9 \leq T \leq 50$  K), indicating a negative magnetoresistance (NMR). Figures 8(a) and (b) show the  $H$  dependence of  $\rho_a$  for Bi-MG with  $2 \leq T \leq 50$  K, where  $H \perp c$  and the field direction is perpendicular to the current direction. For each  $T$ ,  $\rho_a$  decreases with increasing  $H$  at low  $H$  ( $H \geq 100$  Oe), exhibits a local minimum around  $H = 2.5$  kOe, and increases with further increasing  $H$ . The sign of the difference  $\Delta\rho_a [= \rho_a(T, H) - \rho_a(T, H = 0)]$  is negative for  $0 \leq H \leq 3.5$  kOe due to the possible 2D weak localization effect (WLE).<sup>30</sup> It changes from negative to positive at  $H = 3.5$  kOe. The resistivity  $\rho_a$  drastically increases with further increasing  $H$ , as is observed in compensated metals such as bulk Bi.<sup>31</sup> The  $H$  dependence of  $\rho_a$  for  $3 \text{ kOe} \leq H \leq 45 \text{ kOe}$  can be well described by  $\rho_a = \rho_0 + \rho_1 H + \rho_2 H^2$ , where  $\rho_0$ ,  $\rho_1$ , and  $\rho_2$  are constants:  $\rho_0 = 4.290 \text{ m}\Omega\text{cm}$ ,  $\rho_1 = (9.85 \pm 0.11) \times 10^{-3} \mu\Omega\text{cm}/\text{Oe}$ , and  $\rho_2 = (4.56 \pm 0.23) \times 10^{-8} \mu\Omega\text{cm}/\text{Oe}^2$  at 1.9 K. The linear term ( $\rho_1 H$ ) is dominant compared to the squared-power term ( $\rho_2 H^2$ ) for  $H \ll H_1$ , where  $H_1 = \rho_1/\rho_2 = 216 \text{ kOe}$  at 1.9 K. For comparison, we also measured the  $H$  dependence of  $\rho_a$  in Bi-MG for  $1.9 \leq T \leq 30$  K, where  $H \parallel c$ . At each  $T$ ,  $\rho_a$  increases with increasing  $H$ . Thus

the sign of  $\Delta\rho_a$  is always positive for  $0 < H \leq 47.5 \text{ kOe}$  and  $1.9 \leq T \leq 50 \text{ K}$ , indicating an anti-localization effect which is similar to that observed in Bi thin films<sup>32</sup> with strong spin-orbit interactions.

The  $T$  dependence of  $\rho_a$  at  $H = 45 \text{ kOe}$  for  $H \perp c$  is described by

$$\rho_a = a_0 - a_1 \ln(T), \quad (3)$$

for  $1.9 \leq T \leq 4.3 \text{ K}$ , where  $a_0 = (4.8261 \pm 0.0002) \text{ m}\Omega\text{cm}$  and  $a_1 = (3.79 \pm 0.19) \times 10^{-3} \text{ m}\Omega\text{cm}$ . As shown in previous papers,<sup>12,33</sup> the theory of the 2D WLE predicts that the following relation is valid for the ratio  $a_2/a_1$ ,

$$\frac{a_1}{a_0} = \frac{e^2}{2\pi^2\hbar} \frac{A}{\sigma_{2D}^0}, \quad (4)$$

with  $A = \alpha p + \gamma$ , where  $e^2/(2\pi^2\hbar) = 1.23314 \times 10^{-5} \Omega^{-1}$  and  $\sigma_{2D}^0$  is the in-plane conductivity defined by  $I_c/\rho_a^0$  ( $\rho_a^0$  is the in-plane resistivity and  $I_c$  is the  $c$  axis repeat distance). In the parameter  $A$ ,  $\alpha$  is nearly equal to unity,  $p$  is the exponent of the inelastic life time  $\tau_e$  of the conduction electrons ( $\tau_e \approx T^{-p}$ ), and  $\gamma$  is a numerical factor giving a measure of the screening by other carriers. For convenience, here we use the value of  $\sigma_{2D}^0$  ( $= 1.89 \times 10^{-2} \Omega^{-1}$ ) for kish graphite ( $I_c = 3.35 \text{ \AA}$  and  $\rho_a^0 = 1.77 \mu\Omega\text{cm}$  at  $T = 4.2 \text{ K}$ ) obtained by Koike et al.,<sup>27</sup> instead of the corresponding data for Bi-MG. A kish graphite is a high-quality single crystal of graphite which is deposited on walls of blast furnaces for steel production. Using  $a_1/a_0 = 7.853 \times 10^{-4}$  the parameter  $A$  is estimated as  $A = 1.20$ , which is comparable with 1.14 for stage-4  $\text{MoCl}_5$  GIC.<sup>33</sup> These results suggest that the logarithmic behavior of  $\rho_a$  can be explained in terms of the 2D WLE.

#### E. Field induced metal-semiconductor transition

In Fig. 9(a) we show the  $T$  dependence of the difference ( $\mu_a$ ) between  $\rho_a$  at  $T$  and that at 20 K for various  $H$  ( $H \perp c$ ):  $\mu_a = \rho_a(T, H) - \rho_a(T = 20 \text{ K}, H)$ . The  $T$  dependence of  $\mu_a$  below 10 K is dependent on  $H$ . The difference  $\mu_a$  shows a metallic behavior ( $d\mu_a/dT > 0$ ) below 15 - 20 kOe, while it shows a semiconductor-like behavior ( $d\mu_a/dT < 0$ ) above  $H = 25 \text{ kOe}$ . In Fig. 9(b) we show the  $T$  dependence of  $\mu_a$  for  $H \parallel c$ . The  $T$  dependence of  $\mu_a$  below 7 K is dependent on  $H$ . The difference  $\mu_a$  shows a metallic behavior ( $d\mu_a/dT > 0$ ) below 10 kOe, while it shows a semiconductor-like behavior above 20 kOe. Note that  $\mu_a$  at  $H = 47.5 \text{ kOe}$  drastically increases with decreasing  $T$ , leading to the insulating state. The magnitude of  $\mu_a$  for  $H \parallel c$  is on the same order as that for  $H \perp c$ . The  $T$  dependence of  $\rho_a$  at  $H = 47.5 \text{ kOe}$  for  $H \parallel c$  is well described by Eq.(3) for  $1.9 \leq T \leq 4.3 \text{ K}$ , where  $a_0 = (5.8385 \pm 0.0002) \text{ m}\Omega\text{cm}$  and  $a_1 = (5.33 \pm 0.23) \times 10^{-3} \text{ m}\Omega\text{cm}$ . The corresponding fitting curve is denoted by the solid line in the inset of Fig. 9(b). The ratio  $a_1/a_0 = 9.13 \times 10^{-4}$  is almost the same as that ( $=$

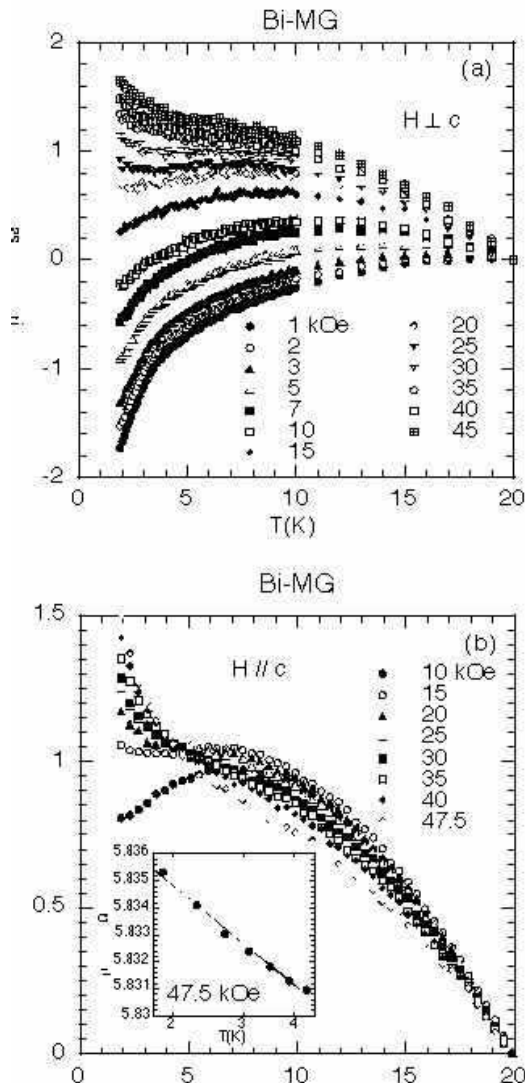


FIG. 9:  $T$  dependence of the difference  $\mu_a$  between  $\rho_a(T, H)$  and  $\rho_a(T = 20\text{K}, H)$  [ $\mu_a = \rho_a(T, H) - \rho_a(T = 20\text{K}, H)$ ] for Bi-MG with various  $H$  ( $1 \leq H \leq 45$  kOe).  $I \perp H$ . (a)  $H \perp c$ . (b)  $H \parallel c$ . The inset of (b) shows the  $T$  dependence of  $\rho_a(T, H)$  at  $H = 47.5$  kOe. The solid line denotes the fitting curve of the data to Eq.(3).

$7.85 \times 10^{-4}$ ) for  $\rho_a$  at  $H = 45$  kOe for  $H \perp c$  (see Sec. III C), indicating the occurrence of 2D WLE.

Bi-MG undergoes a transition from the metallic phase to the semiconductor-like phase at a critical field  $H_c$ . Similar crossover behavior is observed in Si MOSFET,<sup>3</sup> and amorphous metal films of  $\text{InO}_x$ ,<sup>5</sup> MoGe,<sup>7</sup> and Bi.<sup>8</sup> The value of  $H_c$  ( $\approx 25$  kOe) for Bi-MG is almost the same as that for Si MOSFET<sup>3</sup> and amorphous MoGe film.<sup>7</sup> Note that the Zeemann energy  $gS\mu_B H$  at 25 kOe corresponds to a thermal energy  $k_B T_H$  with  $T_H = 1.7$  K, where  $g = 2$  and  $S = 1/2$ . The temperature  $T_H$  is slightly lower than  $T_c$  ( $= 2.48$  K) for the superconductivity. The suppression of the metallic phase by  $H$  is independent of the directions of  $H$  ( $H \parallel c$  and  $H \perp c$ ) for Bi-MG. These results suggest that the spin related effect is significant compared to the orbital effect. This is consistent with the result derived from the susceptibility measurement that the Curie-like susceptibility is dominant at low  $T$ .

#### IV. CONCLUSION

Bi-MG shows superconductivity at  $T_c = 2.48$  K, where the coherence length is much larger than the size of nanoparticles. The spin related effect characterized by a Curie-like susceptibility is enhanced, while the orbital effect is greatly suppressed. The transition from metallic phase to semiconductor-like phase is induced by the application of  $H$  above 25 kOe. A negative magnetoresistance in  $\rho_a$  and a logarithmic divergence of  $\rho_a$  with decreasing  $T$  are indicative of the 2D WLE.

#### Acknowledgments

We would like to thank Kikuo Harigaya for valuable comments on the magnetism of nanographites with zigzag edges. The work at SUNY-Binghamton was supported by SUNY-Research Foundation (Grant No. 240-9522A). The work at Osaka University was supported by the Ministry of Cultural Affairs, Education and Sport, Japan under the grant for young scientists (No. 70314375) and by Kansai Invention Center, Kyoto, Japan. We were grateful to Advanced Ceramics Corporation, Ohio for providing us with HOPG (grade ZYA).

\* suzuki@binghamton.edu

<sup>1</sup> E. Abrahams, P.W. Anderson, D.C. Licciardello, and T.V. Ramakrishnan, Phys. Rev. Lett. **42**, 673 (1979).  
<sup>2</sup> S.V. Kravchenko, W.E. Mason, G.E. Bowker, J.E. Furneaux, V.M. Pudalov and M. D'Iorio, Phys. Rev. B **51**, 7038 (1995).  
<sup>3</sup> D. Simonian, S.V. Kravchenko, M.P. Sarachik, and V.M. Pudalov, Phys. Rev. Lett. **79**, 2304 (1997).  
<sup>4</sup> S.V. Kravchenko and T.M. Klapwijk, Phys. Rev. Lett. **84**, 2909 (2000).

<sup>5</sup> A.F. Hebard and M.A. Paalanen, Phys. Rev. Lett. **65**, 927 (1990).  
<sup>6</sup> Ali Yazdani and A. Kapitulnik, Phys. Rev. Lett. **74**, 3037 (1995).  
<sup>7</sup> N. Mason and A. Kapitulnik, Phys. Rev. Lett. **82**, 5341 (1999).  
<sup>8</sup> N. Markovic, C. Christiansen, and A.M. Goldman, Phys. Rev. Lett. **81**, 5217 (1998).  
<sup>9</sup> J. Walter, H. Shioyama, and Y. Sawada, Carbon **36**, 1811 (1998).



- <sup>10</sup> J. Walter and H. Shioyama, Carbon **37**, 1151 (1999).
- <sup>11</sup> E. McRae and J. Walter, Carbon **39**, 717 (2001).
- <sup>12</sup> M. Suzuki, C.Lee, I.S. Suzuki, K. Matsubara, and K. Sugihara, Phys. Rev. B **54**, 17128 (1996).
- <sup>13</sup> M. Fujita, K. Wakabayashi, K. Nakada, and K. Kusakabe, J. Phys. Soc. Jpn. **65**, 1920 (1996).
- <sup>14</sup> K. Wakabayashi, M. Sigrist, and M. Fujita, J. Phys. Soc. Jpn. **67**, 2089 (1998).
- <sup>15</sup> K. Wakabayashi, M. Fujita, H. Ajiki, and M. Sigrist, Phys. Rev. B **59**, 8271 (1999).
- <sup>16</sup> J. Walter and H. Shioyama, Phys. Lett. A **254**, 65 (1999).
- <sup>17</sup> J. Walter, Adv. Mater. **12**, 31 (2000).
- <sup>18</sup> J. Walter, Phil. Mag. Lett. **80**, 257 (2000).
- <sup>19</sup> D.B. Haviland, Y. Liu, and A.M. Goldman, Phys. Rev. Lett. **18**, 2180 (1989).
- <sup>20</sup> B. Weitzel and H. Micklitz, Phys. Rev. Lett. **66**, 385 (1991).
- <sup>21</sup> G. Deutscher, O. Entin-Wohlman, and Y. Shapira, Phys. Rev. B **22**, 4264 (1980).
- <sup>22</sup> D. Saint-James and P.G. de Gennes, Phys. Lett. **7**, 306 (1963).
- <sup>23</sup> S. Tanuma, in *Graphite Intercalation Compounds II*, edited by H. Zabel and S.A. Solin (Springer-Verlag, Berlin, 1992) p.163.
- <sup>24</sup> A. Fukunaga, S. Chu, and M.E. McHenry, J. Mater. Res. **13**, 2465 (1998).
- <sup>25</sup> O.E. Andersson, B.L.V. Prasad, H. Sato, T. Enoki, Y. Hishiyama, Y. Kaburagi, M. Yoshikawa, and S. Bandow, Phys. Rev. B **58**, 16387 (1998).
- <sup>26</sup> Y. Shibayama, H. Sato, T. Enoki, and M. Endo, Phys. Rev. Lett. **84**, 1744 (2000).
- <sup>27</sup> Y. Koike, S. Morita, T. Nakamoto, and T. Fukase, J. Phys. Soc. Jpn. **54**, 713 (1985).
- <sup>28</sup> W. Zwerger, in *Quantum Coherence in Mesoscopic Systems*, edited by B. Kramer (Plenum Press, New York, 1991) p.491.
- <sup>29</sup> Y. Liu, D.B. Haviland, L.I. Glazman, and A.M. Goldman, Phys. Rev. Lett. **68**, 2224 (1992).
- <sup>30</sup> S. Hikami, A.I. Larkin, and Y. Nagaoka, Prog. Theor. Phys. **63**, 707 (1980).
- <sup>31</sup> M. Suzuki and S. Tanuma, J. Phys. Soc. Jpn. **45**, 1645 (1978).
- <sup>32</sup> F. Komori, S. Kobayashi, and W. Sasaki, J. Phys. Soc. Jpn. **52**, 368 (1983).
- <sup>33</sup> M. Suzuki, I.S. Suzuki, K. Matsubara, and K. Sugihara, Phys. Rev. B **61**, 5013 (2000).